Ultrasound in Med. & Biol., Vol. 25, No. 5, pp. 823–830, 1999
Copyright © 1999 World Federation for Ultrasound in Medicine & Biology
Printed in the USA. All rights reserved
0301-5629/99/$–see front matter

PII S0301-5629(99)00026-5

● *Original Contribution*

COMPUTATIONAL METHODS FOR ULTRASONIC BONE ASSESSMENT

GANGMING LUO,[†] JONATHAN J. KAUFMAN,[‡]* ALESSANDRO CHIABRERA,[§] BRUNO BIANCO,[§] JOHN H. KINNEY,[‖] DAVE HAUPT,[‖] JAMES T. RYABY[¶] and ROBERT S. SIFFERT*

[†]New York Department of Veterans Affairs Medical Center and Department of Rehabilitation Medicine, New York University Medical Center, New York, NY, USA; [‡]CyberLogic, Inc., New York, NY, USA; *Department of Orthopedics, The Mount Sinai School of Medicine, New York, NY USA; [§]Department of Biophysical and Electronic Engineering, University of Genoa, Genoa, Italy; [‖]Department of Materials Science, Lawrence Livermore National Laboratories, Livermore, CA, USA; and [¶]OrthoLogic Corp., Tempe, AZ, USA

(*Received* 7 *December* 1998; *in final form* 18 *February* 1999)

Abstract—Ultrasound has been proposed as a means to noninvasively assess bone and, particularly, bone strength and fracture risk. Although there has been some success in this application, there is still much that is unknown regarding the propagation of ultrasound through bone. Because strength and fracture risk are a function of both bone mineral density and architectural structure, this study was carried out to examine how architecture and density interact in ultrasound propagation. Due to the difficulties inherent in obtaining fresh bone specimens and associated architectural and density features, simulation methods were used to explore the interactions of ultrasound with bone. A sample of calcaneal trabecular bone was scanned with micro-CT and subjected to morphological image processing (erosions and dilations) operations to obtain a total of 15 three-dimensional (3-D) data sets. Fifteen two-dimensional (2-D) slices obtained from the 3-D data sets were then analyzed to evaluate their respective architectures and densities. The architecture was characterized through the fabric feature, and the density was represented in terms of the bone volume fraction. Computer simulations of ultrasonic propagation through each of the 15 2-D bone slices were carried out, and the ultrasonic velocity and mean frequency of the received waveforms were evaluated. Results demonstrate that ultrasound propagation is affected by both density and architecture, although there was not a simple linear correlation between the relative degree of structural anisotropy with the ultrasound measurements. This study elucidates further aspects of propagation of ultrasound through bone, and demonstrates as well as the power of computational methods for ultrasound research in general and tissue and bone characterization in particular. **© 1999 World Federation for Ultrasound in Medicine & Biology.**

Key Words: **Computational methods, Ultrasound simulation, Trabecular bone, Bone mineral density, Architecture, Fabric, Ultrasound velocity, Mean frequency, Anisotropy.**

INTRODUCTION

Ultrasound is currently being investigated as a means of noninvasively assessing bone. It has been suggested that, because ultrasound is a mechanical wave, it may be able to evaluate additional factors related to bone strength in comparison to bone density alone (Kaufman and Einhorn 1993). For example, it is known that architectural structure is an important aspect in osteoporotic fractures (Parfitt 1987). In addition, although bone mass accounts for up to 65% of the variation in bone strength, architecture, when characterized by a feature known as fabric, can explain up to an additional 30% (Turner and Cowin 1987; Turner et al. 1988; Van Reitbergen et al. 1998). A study on adaptive bone remodeling has shown that architecture is needed to specify the biomechanical properties of trabecular bone (Siffert et al. 1996). It has also been recently reported in a clinical study that the relative degree of anisotropy of trabecular bone is independently (of bone mass) associated with an increase of fracture incidence (Wenzel et al. 1998).

The primary method currently used for clinical bone assessment is based on x-ray absorptiometry, and measures total bone mass (often normalized to the area over which the mass measurement is made in units of g/cm^2) at a particular anatomic site (Ott et al. 1987). Because other factors, such as architecture, also appear to have a role in determining an individual's risk of fracture, ultrasound is one alternative that has generated much at-

Address correspondence to: Jonathan J. Kaufman, Ph.D., CyberLogic, Inc., 611 Broadway, Suite 707, New York, NY 10012 USA. E-mail: jjkaufman@cyberlogic.com

tention (Alves et al. 1996b; Gluer et al. 1997). In addition to their potential for conveying architectural aspects of bone, ultrasonic techniques also would have advantages as "pure" bone densitometers, in view of their use of nonionizing radiation and inherently lower costs, compared with x-ray densitometric methods. Although ultrasonic methods appear promising for noninvasive bone assessment, they have not yet fulfilled their potential.

Presently, ultrasonic techniques are capable of explaining about 70% of the variability in observed bone density (Gluer et al. 1997). Part of the reason for this is the fact that ultrasound seems to be affected, not only by how much bone is contained along the propagation pathway, but also by how that bone is organized in terms of its microstructure or architecture (Gluer et al. 1993; Turner and Eich 1991). Thus, the variability of trabecular bone architecture may affect ultrasound propagation and, therefore, may make accurate density determination difficult using present ultrasound technology. In an analogous fashion, the variability of trabecular bone with respect to architecture also results in an inability to accurately estimate trabecular bone strength using current ultrasound methodology, at least in comparison to estimates based on bone mass only (Turner and Eich 1991).

The long-term objective of this research is to make ultrasound an accurate and precise tool for clinical assessment of bone density, bone strength and fracture risk. The specific goal of this study was to elucidate the interaction and combined effects that trabecular bone density and architecture have on transmission ultrasound measurements. A second objective of the study was to demonstrate to the scientific and engineering community the usefulness of computational methods in furthering research and development in ultrasound in general, and in tissue and bone characterization in particular.

MATERIALS AND METHODS

A human calcaneus, from which all soft tissue had been previously removed, was obtained from a commercial supplier. A cylindrical core 1.42 cm in diameter was cut from the posterior portion of the calcaneus in the medial-lateral direction, using an electric drill corer. The cortical shells were then removed using a rotating disk cutter to produce a 10.3-mm long cylindrical sample of calcaneal trabecular bone. The specimen was three-dimensionally imaged using microCT according to a protocol described elsewhere (Kinney and Nichold 1992) and the data reconstructed in cubic volume elements (voxels) that were 33.4 μm on edge.

The three-dimensional (3-D) image data corresponding to the trabecular bone cylinder was then processed using sequences of morphological image processing operations (Serra 1982). The processes of erosion (thinning) and dilation (thickening) were applied in various combinations to obtain bone images in distinct states of densities and architectures. In particular, the original image data was eroded and dilated in 14 distinct erosion and dilation sequences to obtain a total of 15 distinct 3-D images (the original plus 14 transformed images). The distinct sequences of erosions and dilations were chosen so that the changes induced on the original specimen might mimic those seen under osteoporosis (Luo et al. 1999); the morphological operations used the classical erosion and dilation operators (Russ 1995). An arbitrarily selected two-dimensional (2-D) slice was then extracted from each of the 15 3-D data sets to obtain a total of 15 2-D images. Each of the 15 2-D images was then analyzed for volume fraction and fabric anisotropy. Volume fraction was defined simply as the proportion of the total image area occupied by bone and, thus, varied between 0 and 1. It is directly analogous to bone mineral density, apart from an unimportant (for our purposes) constant scale factor. (It should be pointed out that bone mineral density as we have described it here is often referred to as "apparent density," which is also distinct from the "areal" bone mineral density measured by most current clinical x- ray bone densitometers. To minimize confusion, our results will be related to the dimensionless quantity "bone volume fraction.") The method for computing the architectural fabric of trabecular bone has been described in detail elsewhere (Odgaard et al. 1997; Siffert et al. 1996; Whitehouse 1974). Briefly, each 2-D image was analyzed in terms of the mean intercept length (MIL) (*i.e.*, the average length of void region) as a function of angle of orientation. The MIL was plotted on a polar coordinate plot and the relative degree of anisotropy (RDA) of the 2-D trabecular bone structure was computed. In particular, the RDA was defined as the ratio of the MIL in the principal direction of the trabeculae (*i.e.*, the angle at which the MIL is maximum) to the MIL in the direction orthogonal to the principal direction (Fig. 1).

Next, computer simulations of ultrasound propagation through each of the 15 2-D images were carried out using a computer software package (Wave2000, CyberLogic, Inc., New York, NY). Wave2000 simulates the complete solution to the 2-D elastic wave equation:

$$\rho \frac{\partial^2 w}{\partial t^2} = \left(\mu + \eta \frac{\partial}{\partial t}\right) \nabla^2 w + \left(\lambda + \mu + \phi \frac{\partial}{\partial t}\right) \nabla(\nabla \cdot w). \quad (1)$$

In eqn (1), ρ is the volumetric density in kg/m^3 of each material *per se*, λ and μ are the first and second Lamé

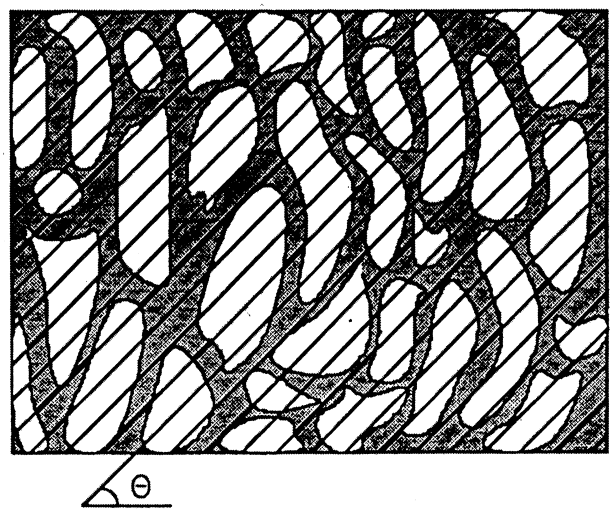

Fig. 1. Test lines superimposed on a cancellous bone specimen. The test lines are oriented at the angle θ. The mean intercept length measured at this angle is denoted by MIL(θ).

constants, respectively, in units of N/m2, η and ϕ are the first and second viscosities in units of $N-s/m^2$, and $w = w(x,y,t)$ is the displacement vector as a function of Cartesian coordinates x and y and of time t. Wave2000 implements a finite difference (FD) solution to eqn (1), and is based on a local interaction formulation designed for parallel processing implementation, as presented by Delsanto et al. (1994) for the lossless case. Wave2000 implements an extension of this formulation, which allows for viscous losses (attenuation) and execution on a standard personal computer (PC) running Microsoft Windows® 95, 98 or NT.

The simulations were carried out with the following set of conditions. For the bone portions of the interrogated sample, $\rho = 1850$ kg/m^3, $\lambda = 9306$ MPa, $\mu = 3127$ MPa, $\eta = 40$ Pa·s, $\phi = 0.1$ Pa·s. This produced longitudinal and shear (phase) velocities at 1 MHz of 2900 m/s and 1303 m/s, and differential specific attenuations of 4.1 dB cm^{-1} MHz^{-1} and 33.5 dB cm^{-1} MHz^{-1}, respectively. The material in the marrow spaces of the tissue was assumed to be fresh blood. For this case, $\rho = 1055$ kg/m^3, $\lambda = 2634$ MPa, $\mu = 0$ Mpa, $\eta = 0.1$ Pa·s, $\phi \approx 0$ Pa·s. This produced longitudinal and shear (phase) velocities at 1 MHz of 1580 m/s and 34.5 m/s, and differential specific attenuations of 0.11 dB cm^{-1} MHz^{-1} and 7905 dB cm^{-1} MHz^{-1}, respectively. A 1-MHz sine wave with a Gaussian envelope was used as the source waveform in all cases (Fig. 2). The source and receiver were operated in through transmission mode; each was 14-mm long and extended over the entire respective opposite sides of the 2-D image. The receiver

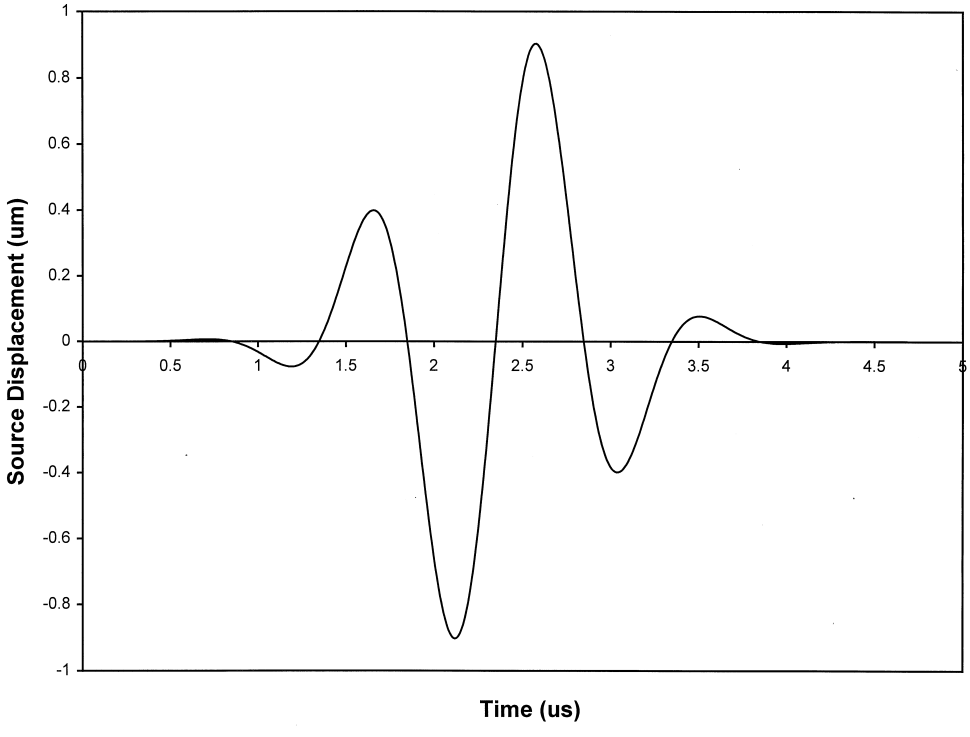

Fig. 2. A 1-MHz sine wave with a Gaussian envelope, which served as the excitation waveform in all of the simulations.

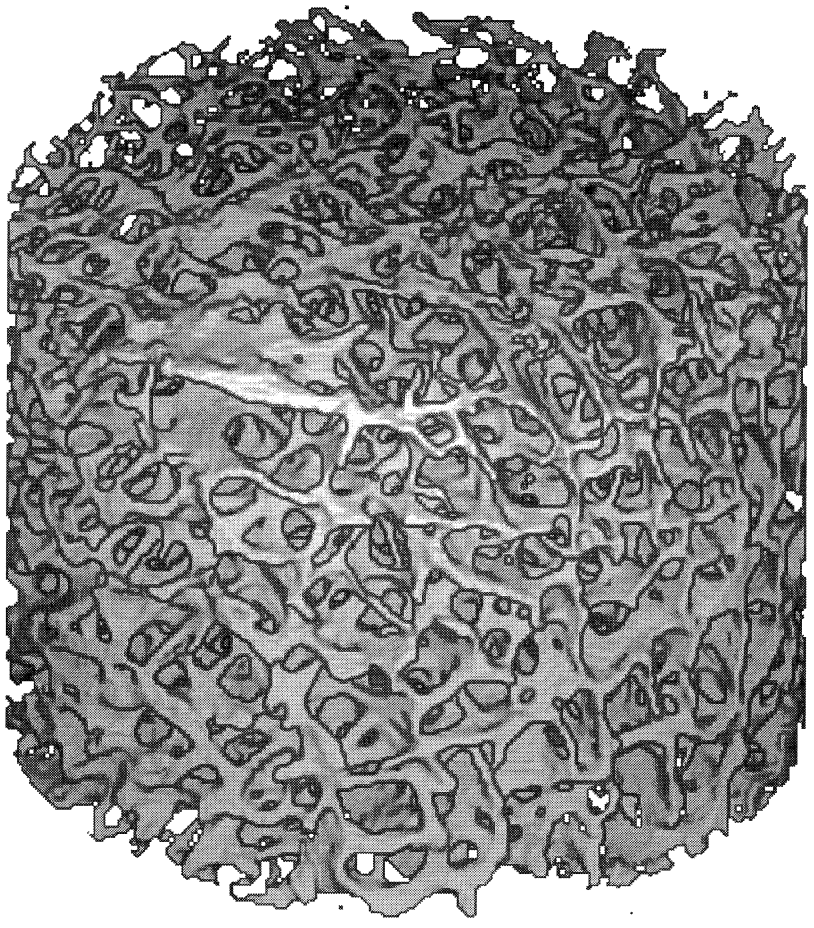

Fig. 3. The 3-D-rendered image of the original calcaneal bone sample.

computed the average or mean displacement along its defined length. The simulations were carried out with the source-receiver pair in one of two orientations. The first was done with the transducer pair aligned along the main trabecular orientation ("∥"). The second was done with the transducer pair aligned orthogonal to the main trabecular orientation ("⊥"). The image was initially rotated to achieve the desired alignment. Receiver measurements were then computed (*i.e.*, simulated) for each of the 15 samples in each of the two directions, for a total of 30 receiver waveforms. The ultrasound velocities (UVs) in the parallel and orthogonal directions ($UV_{\parallel}$ and $UV_{\perp}$, respectively) and mean frequencies (MFs) in the parallel and orthogonal directions ($MF_{\parallel}$ and $MF_{\perp}$, respectively) were computed for each of the received waveforms. The ultrasound velocities were determined using a transit time technique (Alves et al. 1996a). The mean frequencies were computed by counting zero crossings of the received waveform, and dividing by twice the time over which the zero-crossings occurred (Kedem 1994). The MF is related to the attenuation coefficient (*i.e.*, an increase in attenuation usually implies a decrease in the MF), but has been shown to be more robust and not as subject to artefacts as a linear estimate of the attenuation slope in clinical bone measurements (Kaufman et al. 1996). Mean frequency anisotropy (MFA) and ultrasound velocity anisotropy (UVA), analogous to the definition of the RDA, were defined by

$$MFA = \frac{MF_{\parallel}}{MF_{\perp}} \tag{2}$$

and

$$UVA = \frac{UV_{\parallel}}{UV_{\perp}}. \tag{3}$$

Finally, univariate and multivariate least squares regression analyses were carried out with respect to the ultra-

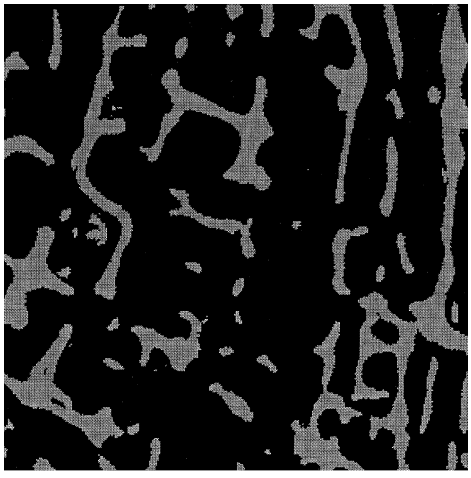

a

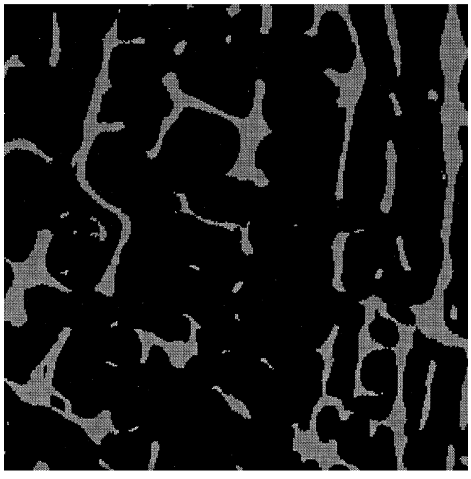

b

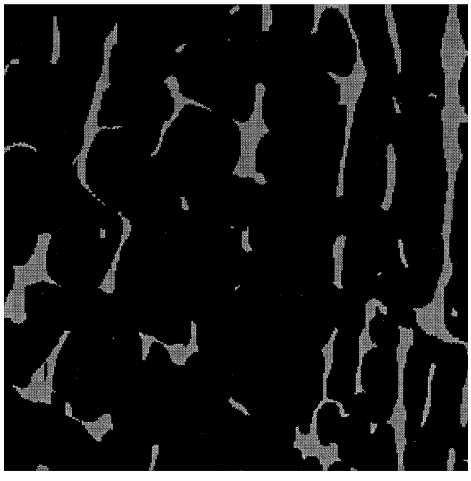

c

Fig. 4. (a) A single slice from the original calcaneal bone sample. (b) A single slice from an image that had two erosions applied to the original calcaneal bone sample. (c) A single slice from an image that had four erosions applied to the original calcaneal bone sample.

sound features, volume fraction and fabric anisotropy, and the R^2 values evaluated (Bethea and Rhinehart 1991).

RESULTS

The 3-D image of the calcaneal bone cylinder as determined by microCT is shown in Fig. 3. Three microCT image slices are shown in Fig. 4a–c. The first is a slice from the original image (without any dilations or erosions) and the other two are slices associated with two and four erosions, respectively. These three images have volume fractions of 0.21, 0.15 and 0.11 and architectural fabric anisotropies (*i.e.*, RDAs) of 1.42, 1.58 and 2.07, respectively. Table 1 provides data on the entire set of 15 2-D images, as well as information on the specific sequence of erosions (denoted by "E") and dilations (denoted by "D") used to obtain the data set. The mean volume fraction of the 15 bone slices was 0.162, and ranged from a minimum of 0.105 to a maximum of 0.210. The mean RDA was 1.84, and ranged from a minimum of 1.42 to a maximum of 2.35.

Figure 5a shows an instantaneous "snapshot" of a propagating ultrasound wave within the slice of Fig. 4a. As may be seen, there is a significant amount of scattering associated with propagation of the ultrasound wave. The simulated receiver measurements associated with the same sample along the principal and orthogonal directions are shown in Fig. 5b and c, respectively.

Plots of all the 30 UVs and MFs vs. volume fractions are shown in Fig. 6a and b, respectively. Note that different symbols are used to denote propagation in the direction parallel (□) and orthogonal (●) to the primary orientation of the trabeculae, respectively. Linear correlation analyses with volume fraction for the two individual velocity curves of Fig. 6a (*i.e.*, the parallel and orthogonal data sets), resulted in R^2 values of 0.98 ($p < 0.0001$) and 0.96 ($p < 0.0001$), respectively. Linear correlation analyses with volume fraction for the two individual mean frequency curves of Fig. 6b (*i.e.*, the parallel and orthogonal data sets) resulted in R^2 values of 0.91 ($p < 0.0001$) and 0.90 ($p < 0.0001$), respectively.

Linear correlation analyses were also carried out on the ultrasound data without regard to orientation, that is, with the data grouped together so that there were 30 data points instead of 15 for the mean frequency and velocity linear regressions. Combining the parallel and orthogonal mean frequency data and correlating the 30 data points with volume fraction resulted in an R^2 value of 0.29 ($p < 0.01$). Combining the parallel and orthogonal velocity data and correlating the 30 data points with volume fraction resulted in an R^2 value of 0.85 ($p < 0.0001$).

Next, correlation analysis of the ultrasound data with respect to the architectural characteristic of the 2-D

Table 1. Summary of data for the 15 s-D slices associated with the 15 3-D data sets of the calcaneal bone sample.

Sample #	VF	RDA	$UV_{\parallel}$ (m/s^{-1})	$UV\perp$ (m/s^{-1})	$MF_{\parallel}$ (kHz)	$MF\perp$ (kHz)	UVA	MFA
1 (original)	0.210	1.42	1802	1858	820	704	0.969	1.17
2 (E)	0.178	1.48	1753	1800	893	769	0.974	1.16
3 (ED)	0.206	1.52	1800	1853	847	714	0.971	1.19
4 (EE)	0.149	1.58	1713	1747	962	769	0.981	1.25
5 (EED)	0.175	1.58	1757	1792	909	772	0.981	1.18
6 (EEDD)	0.201	1.66	1801	1838	833	694	0.979	1.20
7 (EEE)	0.124	1.81	1658	1705	943	806	0.972	1.17
8 (EEED)	0.145	1.81	1711	1736	962	794	0.986	1.21
9 (EEEDD)	0.166	1.88	1749	1771	909	758	0.988	1.19
10 (EEEDDD)	0.187	1.98	1792	1808	862	714	0.991	1.21
11 (EEEE)	0.105	2.07	1555	1674	980	893	0.929	1.09
12 (EEEED)	0.121	2.06	1651	1698	962	833	0.972	1.16
13 (EEEEDD)	0.138	2.15	1703	1724	943	781	0.988	1.21
14 (EEEEDDD)	0.155	2.24	1740	1747	920	781	0.996	1.18
15 (EEEEDDDD)	0.172	2.35	1769	1779	899	694	0.994	1.30

The listings of Es and Ds in parenthesis indicate the specific sequences of erosions and dilations, respectively, that were used to obtain the given data sets.

trabecular bone slices was carried out. Little correlation was found between the architectural anisotropy (*i.e.*, the RDA) and either of the ultrasound measures of anisotropy, UVA, or MFA. The correlation coefficient between RDA and UVA was $r = 0.11$ and between RDA and MFA was $r = 0.17$. Bivariate linear regressions were used to relate RDA to both $MF_{\parallel}$ and $MF_{\perp}$, as well as to both $UV_{\parallel}$ and $UV_{\perp}$. No significant correlations were found in either case.

DISCUSSION AND SUMMARY

This study has provided information on how density and architecture affect ultrasound propagation. For example, the data showed that ultrasound measurements are affected by the direction in which an ultrasound wave propagates through a bone slice. This is most readily apparent in Fig. 6a and b, because the only difference in the experimental condition for each data pair, that is, for the $\parallel$ and $\perp$ ultrasound features associated with each sample, is the trabecular structure itself, because the volume fraction, transducer characteristics and material properties are unaltered. Previously, both theoretical (Chiabrera et al. 1996) and *in vitro* experimental (Gluer et al. 1993) results have demonstrated that ultrasound propagation is direction-dependent. The present study extends these results by accurately quantifying the architectural fabric and density and relating them to ultrasound measurements. Although fabric anisotropy was not linearly correlated with ultrasound measurements, this information seems to be contained in the measurements owing to the strong dependence of ultrasound measurements on direction of propagation and structure.

The clinical implications of these findings are that, unless bone architecture is accounted for, ultrasound, as measured by either velocity or attenuation-dependent methods (*e.g.*, mean frequency), will not be able to uniquely identify the value of bone mass at a particular anatomical site. In other words, with a standard single element transducer pair used in through transmission, correlations of only about $0.80-0.85$ ($0.64 < R^2 < 0.72$) between ultrasound and bone density may represent an inherent upper limit. Although this degree of linear correlation can be clinically useful (the United States Food and Drug Administration has already approved an ultrasound bone densitometer with this approximate correlation with bone mass), it would nevertheless be highly advantageous to be able to improve upon this limitation. The data suggests that one way to achieve such an improvement is to incorporate ultrasound measurements having more than one direction of propagation. Further work utilizing array-based methods may be an approach by which this may be accomplished (Kaufman et al. 1998). It is also interesting to note that the greatest difference in velocity occurred at the smallest value of volume fraction, suggesting that architectural characteristics may play the most confounding role in cases of primary clinical interest, namely in osteoporotic subjects.

It is well known that trabecular bone is extremely heterogeneous (Keaveny and Hayes 1993). Thus, small changes in positioning of an ultrasound transducer pair as, for example at the heel, can produce large changes in the received ultrasound waveform. These changes occur at least in part because of variations of the acoustic pathway in terms of its total bone mass and/or architectural structure. To correctly identify bone mass and strength, it will be necessary to develop methods that are affected at least somewhat independently by both aspects, by architecture and density. As one, perhaps ob-

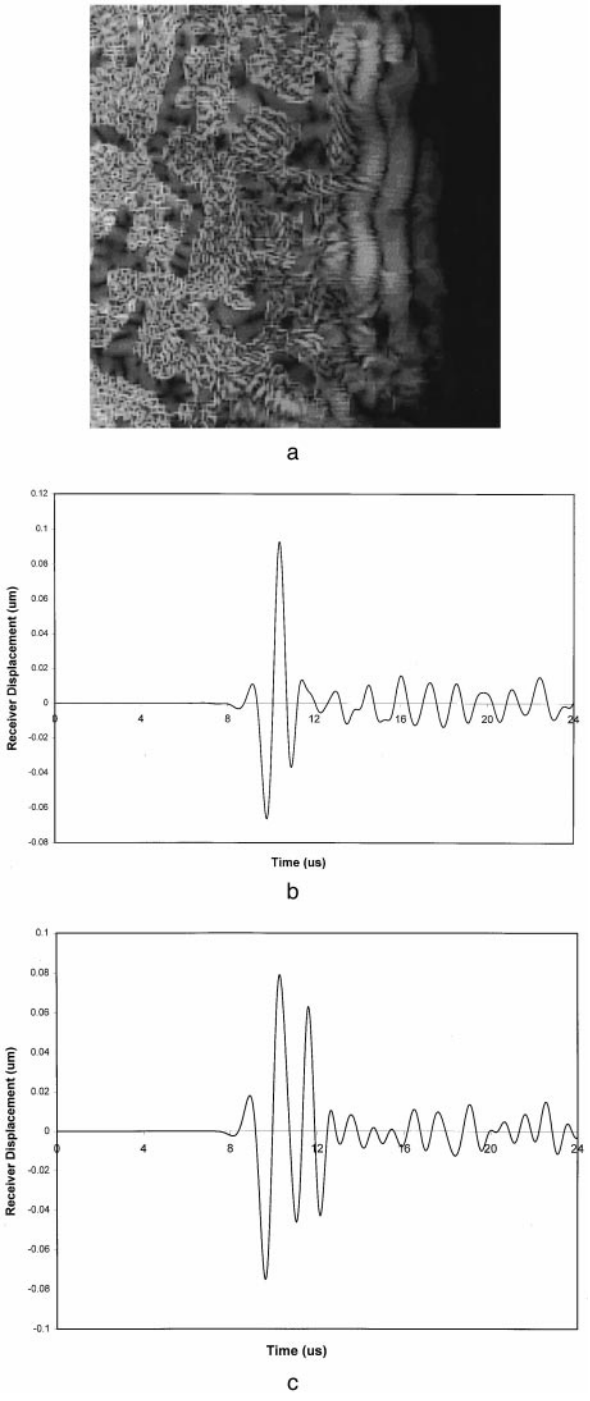

Fig. 5. (a) An instantaneous "snapshot" at $t = 7.4$ s of an ultrasound wave propagating (from left to right) through the 2-D bone slice shown in Fig. 4a, in the direction orthogonal to the main trabecular orientation. The grey level of the image is proportional to the magnitude of the material displacement at each point in the trabecular bone slice. (b) The simulated received waveform propagated along the principal direction of the trabeculae for the structure represented by Fig. 4a. (c) The simulated received waveform propagated orthogonal to the principal direction of the trabeculae for the structure represented by Fig. 4a.

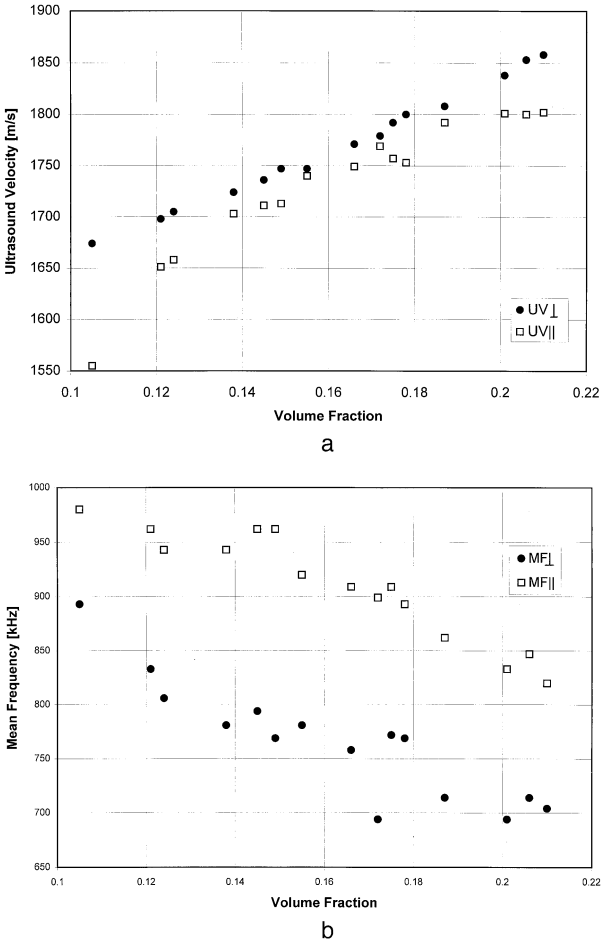

Fig. 6. (a) Plot of ultrasonic velocity (UV) vs. bone volume fraction (VF). (b) Plot of mean frequency (MF) vs. bone volume fraction (VF).

vious, example, the combination of x-ray densitometric with ultrasonic data can perhaps provide the best approach for identifying both density and architecture and, ultimately, bone strength and fracture risk. As another alternative, because age is correlated with bone density, combining age with ultrasound measurements may also be a useful (and extremely simple) approach to enhance ultrasound based density estimation (Kaufman et al. 1996). It is also useful to explore nonlinear combinations of ultrasound and other features (*e.g.*, density, age, weight, height), as well as nonlinear combinations of the ultrasound features themselves, as a means to estimate bone strength and fracture risk. This can be pursued, for example, with neural networks (Kaufman et al. 1994).

Equally important to the specific results obtained relating to bone are the insights gained into how computational methods can be used to address a variety of issues related to ultrasound propagation. In questions relating to bone tissue characterization, for example, it may often be

problematic to obtain large numbers of specimens with known properties. In such cases, computational methods can be very useful. Further, computational techniques can avoid a variety of experimental artefacts that can obscure specific aspects of interest. For example, in preparing samples for *in vitro* measurements, void regions (*i.e.*, air "pockets") within the specimen often are produced and may significantly affect the ultrasound data. Another example of an unwanted artefact is that of nonparallel surfaces. These and other artefacts can be completely avoided (or controlled) using a computational approach such as described here. Indeed, the effects of varying degrees of nonparallel surfaces, for example, can be evaluated on the same "sample," a difficult if not impossible task in experimental settings. In addition to the above examples, computational methods can be used to study the effects of varying viscosity of the marrow (Lin et al. 1993; Alves et al. 1996a), cortical bone and soft tissue, degree of mineralization, and refraction, diffraction and scattering (Xu and Kaufman 1993; Kaufman et al. 1995). It may also be of interest to examine what effect use of phase-insensitive transducers would have on the velocity and mean frequency measurements; this would also be easy to implement in simulation. Finally, it should be noted that our study has focused exclusively on 2-D bone slices and simulations, due to computational overhead associated with full 3-D simulation; subsequent studies will, however, be necessary to extend our results into three dimensions.

Although computational methods have long been utilized by engineers in other fields, such as electromagnetics and structural analysis, it has not as yet been used in any significant manner by ultrasound researchers. Whether this has been because of lack of availability of suitable software or hardware or because of an inherent bias against simulation it is not known. Nevertheless, the value and utilization of computational methods should increase as more examples of their application are presented. Their use for exploring the effects of architecture and density on ultrasound propagation through bone, as presented here, is one such illustration.

REFERENCES

Alves JM, Ryaby JT, Siffert RS, Magee FP, Kaufman JJ. Influence of marrow on ultrasonic velocity and attenuation bovine trabecular bone. Calcif Tissue Int 1996a;58:362–367.

Alves JM, Xu W, Lin D, Siffert RS, Ryaby JT, Kaufman JJ. Ultrasonic assessment of human and bovine trabecular bone: a comparison study. IEEE Trans Biomed Eng 1996b;43(3):249–258.

Bethea RM, Rhinehart RR. Applied engineering statistics. New York: Marcel Dekker, 1991.

Chiabrera A, Bianco B, Siffert RS, Kaufman JJ. Ultrasound measures both bone mass and architecture: theoretical results for an idealized model of trabecular bone. Trans Orthop Res Soc 1996;21(2):600.

Delsanto PP, Schechter RS, Chaslekis HH, Mignogna RB, Kline R. Connection machine simulation of ultrasonic wave propagation in materials. II: the two-dimensional case. Wave Motion 1994;20: 295–314.

Gluer CC, Wu CY, Genant HK. Broadband ultrasound attenuation signals depend on trabecular orientation: An in vitro study. Osteoporosis Int 1993;3:185–191.

Gluer C-C for the International Quantitative Ultrasound Consensus Group. Quantitative ultrasound techniques for the assessment of osteoporosis: expert agreement on current status. J Bone Min Res 1997;12(8):1280–1288.

Kaufman JJ, Einhorn TE. Review—Ultrasound assessment of bone. J Bone Min Res 1993;8(5):517–525.

Kaufman JJ, Alves M, Siffert RS, Magee FP, Ryaby JT. Ultrasound assessment of trabecular bone density using neural networks. J Bone Min Res 1994;9(Suppl. 1):A204.

Kaufman JJ, Friess SH, Chiabrera A, Sorensen J, Ryaby JT, Siffert RS. Two-dimensional array system for ultrasonic bone assessment. Trans Orthop Res Soc 1998;23(2):966.

Kaufman JJ, Murphy G, Fitzpatrick D, Liu L, Ost M, Alves JM, Magee FP, Ryaby JT, Einhorn TA, Siffert RS, Luckey M. A new ultrasound system for bone assessment. J Bone Min Res 1996;11(Suppl. 1):S241.

Kaufman JJ, Xu W, Chiabrera AE, Siffert RS. Diffraction effects in insertion mode estimation of ultrasonic group velocity. IEEE Trans Ultrason Ferroelec Freq Control 1995;42(2):232–242.

Keaveny TM, Hayes WC. A 20-year perspective on the mechanical properties of trabecular bone. J Biomech Eng 1993;115(4B):534-542.

Kedem B. Time series analysis by higher order crossings. New York: IEEE Press, 1994.

Kinney JH, Nichold MC. X-ray tomographic microscopy using synchrotron radiation. Ann Rev Materials Sci 1992;22:121–152.

Lin D, Xu W, Klein M, Einhorn T, Kaufman JJ, Siffert RS. Effect of physical factors on ultrasound attenuation and velocity in bone. J Bone Min Res 1993;8(Suppl. 1):S319.

Luo GM, Kinney JH, Kaufman JJ, Haupt D, Chiabrera A, Siffert RS. Relationship of plain radiographic patterns to three-dimensional trabecular architecture in the human calcaneus. Osteoporosis Int 1999;9(4) (in press).

Odgaard A, Kabel J, Van Reitbergen B, Dalstra M, Huiskes R Fabric and elastic principal directions of cancellous bone are closely related. J Biomech 1997;30(5):487–495.

Ott SM, Kilcoyne RF, Chestnut C III. Ability of four different techniques of measuring bone mass to diagnose vertebral fractures in postmenopausal women. J Bone Min Res 1987;2:201–210.

Parfitt AM. Trabecular bone architecture in the pathogeneses and prevention of fracture. Am J Med 1987;82(1B):68–72.

Russ JC. The image processing handbook. 2nd ed. Boca Raton, FL: CRC Press 1995.

Serra J. Image analysis and mathematical morphology. Vol. 1. London: Academic Press, 1982.

Siffert RS, Luo GM, Cowin SC, Kaufman JJ. Dynamical relationships of trabecular bone density, architecture and strength in a computational model of osteopenia. Bone 1996;18(2):197–206.

Turner CH, Cowin SC. Dependence of elastic constants of an anisotropic porous material upon porosity and fabric. J Materials Sci 1987;22:3178–3184.

Turner CH, Eich M. Ultrasonic velocity as a predictor of strength in bovine cancellous bone. Calcif Tissue Int 1991;49:116–119.

Turner CH, Rho JY, Ashman RB, Cowin SC. The dependence of elastic constants of cancellous bone upon structural density and fabric. Trans Orthop Res Soc 1988;13:74.

Van Reitbergen B, Odgaard A, Kabel J, Huiskes R Relationships between bone morphology and bone elastic properties can be accurately quantified using high resolution computer reconstructions. J Orthop Res 1998;16(1):23–28.

Wenzel TE, Fyhrie DP, Schaffler MB, Goldstein SA. Variations in three-dimensional cancellous architecture of the proximal femur in hip fracture patients and controls. Trans Orthop Res Soc 1998; 23(1):86.

Whitehouse WJ. The quantitative morphology of anisotropic trabecular bone. J Microscopy 1974;101:153–168.

Xu W, Kaufman JJ. Diffraction correction methods for insertion ultrasound attenuation measurement. IEEE Trans Biomed Eng 1993; 40(6):563–570.